ACS APPLIED MATERIALS & INTERFACES

Research Article

www.acsami.org

Experimental and Theoretical Study of the Influence of the State of Dispersion of Graphene on the Percolation Threshold of Conductive Graphene/Polystyrene Nanocomposites

Evgeniy Tkalya,[†] Marcos Ghislandi,[‡,§] Ronald Otten,[∥] Mustafa Lotya,[#] Alexander Alekseev,[§] Paul van der Schoot,*[,∥,⊥] Jonathan Coleman,[#] Gijsbertus de With,[§] and Cor Koning[†]

[†]Department of Chemical Engineering and Chemistry, Polymer Chemistry Group, Technische Universiteit Eindhoven, P.O. Box 513, 5600 MB Eindhoven, The Netherlands

[‡]CETENE-Centro de Tecnologias Estratégicas do Nordeste, Av. Prof. Luiz Freire 01-CDU, Recife 50740-540, Brazil

[§]Laboratory of Materials and Interface Chemistry, Technische Universiteit Eindhoven, 5600 MB Eindhoven, The Netherlands

[∥]Theory of Polymers and Soft Matter and Eindhoven Polymer Laboratories, Eindhoven University of Technology, P.O. Box 513, 5600 MB Eindhoven, The Netherlands

[⊥]Institute for Theoretical Physics, Utrecht University, Leuvenlaan 4, 3584 CE Utrecht, The Netherlands

[#]School of Physics, Centre for Research on Adaptive Nanostructures and Nanodevices (CRANN), Trinity College Dublin, Dublin 2, Ireland

ABSTRACT: The effect of the dispersed state of graphene is studied as a factor influencing the electrical percolation threshold of graphene/polystyrene nanocomposites. We find the percolation threshold of our nanocomposites, prepared with graphene dispersions with different thermodynamic stabilities, degrees of exfoliation, and size polydispersities, to range from 2 to 4.5 wt %. Connectedness percolation theory is applied to calculate percolation thresholds of the corresponding nanocomposites, based on the premise that size polydispersity of graphene platelets in the corresponding solutions must have a strong influence on it. Theory and experimental results agree qualitatively.

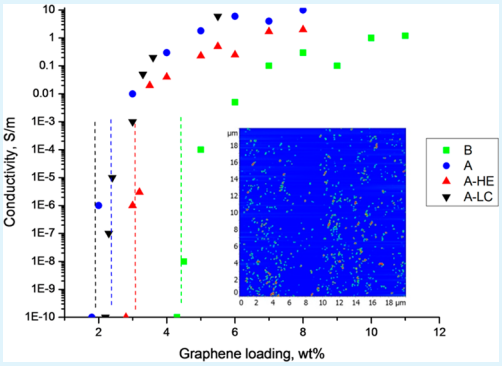

KEYWORDS: *graphene, percolation threshold, polymer nanocomposites*

INTRODUCTION

Graphene is a two-dimensional sheet of sp^2-hybridized carbon. Its extended honeycomb network is the basic building block of other important allotropes; it can be stacked to form three-dimensional graphite, rolled up to form one-dimensional nanotubes, and wrapped to form zero-dimensional fullerenes.[1,2] Polymer nanocomposites based on carbon black, carbon nanotubes (CNTs), and layered silicates have been used for improved mechanical,[3] thermal, electrical, and gas barrier properties of polymers. The discovery of graphene with its combination of extraordinary physical properties and ability to be dispersed in various polymer matrices has created a new class of polymer nanocomposites.[2] At present, a great deal of attention is being paid to the electrical properties of such composites.[2,4−6]

The large variation in the reported percolation threshold values, which range from 0.1 to >2 wt %,[4,7−11] indicates that the dispersion states and other properties of graphene, affected by different processing conditions, must be important in determining the electrical properties of graphene/polymer nanocomposites. For CNT/polymer nanocomposites, the dispersed state of CNTs has been recognized as one of the critical factors governing the conductivity of composites as well as their physical properties. It is generally accepted that well-dispersed CNTs within the polymer matrix enhance the physical properties of the composite. However, a few studies suggest that CNT agglomeration could favor the formation of a percolating network.[12−15] In this work, the dispersed state of graphene in a polystyrene (PS) matrix is discussed as a parameter influencing the percolation threshold of the corresponding composites prepared with the well-known latex technology.[7,16−19] The graphene used in this work was produced from graphite via different methods described well in the literature.[20,21] Analyses indicate these production methods do not yield 100% single-layer graphene, so these materials might present some percentage of few-layer graphene stacked together.

Received: May 23, 2014
Accepted: August 12, 2014
Published: August 12, 2014

EXPERIMENTAL SECTION

Chemicals. Sodium dodecyl sulfate (SDS) (90%, Merck), sodium carbonate (99%, Aldrich), sodium peroxodisulfate (SPS) (90%, Merck), and sodium cholate (SC) (99%, Aldrich) were used as received. Styrene (99%, Merck) was passed over an inhibitor remover column (basic alumina, Aldrich) and distilled under reduced pressure. The inhibitor-free monomers were refrigerated for later use. Water used in all reactions was double deionized water obtained from a purification system. SP-2 graphite from Bay Carbon and natural flake graphite from Branwell Graphite Ltd. (Grade RFL 99.5) were used as provided. Graphene was obtained via a graphite (SP-2 Bay Carbon) oxidation and thermo-expansion process and via graphite (Branwell Graphite Ltd.) exfoliation in a sodium cholate/water solution.[20,21]

Preparation and Characterization of PS Latex. PS latex was synthesized via conventional free radical emulsion polymerization. The reaction was performed at 70 °C with an impeller speed of 400 rpm. The reactor was charged with the following: styrene (252 g), SDS (26 g, 0.09 mol), sodium carbonate (0.7 g, 6.6 mmol), and H_2O (712.2 g). The reaction mixture was degassed by being purged with argon for 30 min. A solution of SPS (0.45 g, 1.9 mmol) in H_2O (10 g) was also degassed. The reaction was started upon the introduction of the initiator solution, and the reaction time was approximately 1 h. The average particle size determined by dynamic light scattering was 90 nm. Size exclusion chromatography analysis showed M_n, M_w, and polydispersity index values of 495 kg mol^{-1}, 944 kg mol^{-1}, and 1.9, respectively.

Preparation of Graphene Dispersions. Exfoliated graphene dispersions from thermally reduced graphite oxide were prepared with the use of a surfactant and energy supplied by ultrasound. The ultrasound was provided by a Sonics Vibracell VC750 horn sonicator with a 10 mm diameter tip. The sonication power was maintained at 100 W during the exfoliation, and the solution was cooled in an ice bath. Volumes were kept under 100 mL to achieve the best sonication for the complete solution. The graphene dispersion made from graphite exfoliated via the liquid-phase exfoliation route was prepared as described previously.[21]

Processing of Composites. The graphene dispersions were mixed with PS latex according to the desired graphene weight percentage in the final composites. A minimum of 10 samples ranging from 0.5 to 12 wt % of graphene were produced for each dispersion. The mixtures were frozen in liquid nitrogen for several minutes, and the frozen water was removed with a Christ Alpha 2-4 freeze-dryer operated at 0.2 mbar and 20 °C overnight. The resulting composite powder was compression molded into films for 20 min at 180 °C between Teflon sheets with a Collin Press 300G instrument.

UV−Vis Spectroscopic Measurements. UV−vis absorption spectra were recorded with a Hewlett-Packard 8453 spectrometer operating between 200 and 1100 nm. Small sample volumes were taken after the sonication process and diluted, resulting in a graphene concentration of 0.0125 mg mL^{-1}. The blank used was the original SC solution, diluted and analyzed under the same conditions that were used for the samples themselves.

Electrical Conductivity Measurements. The electrical conductivity was measured using a standard four-point method. The conductivities of all composite samples were measured for the surface (in-plane) direction. Parallel contact lines 0.5 cm in length with a 0.5 cm interval were drawn with conductive-silver paint (Fluka) on the composite film, and all conductivity measurements were performed at room temperature (25 °C) with a Keithley 6512 programmable electrometer. For each sample, conductivity data represent the average values of 10 consecutive measurements.

Atomic Force Microscopy (AFM) Investigations. The conductive AFM (C-AFM) measurements on composite cross sections were performed with an NTEGRA Tomo instrument (NTMDT Co.). The device is a combination of an EM UC6-NT microtome (Leica) and an SPM measuring head. Such a design allows for alternate microtome cutting and SPM measurements of the sample block face. The local current measurements were performed in C-AFM mode with a gold-coated silicon cantilever (NSC36/Cr-Au, Micromash). The sample was electrically connected to a grounded holder; a bias of 2 V was applied.

Transmission Electron Microscopy (TEM). TEM images were taken using a Sphera type Technai 20 instrument (Fei Co.). This was operated with a 200 kV LaB_6 filament and a bottom-mounted 1024 × 1024 Gatan CCD camera. A carbon-coated gold grid was used.

Raman Spectroscopy. A LABRAM confocal Raman spectroscope equipped with an optical microscope was utilized. Samples were irradiated with a red highly polarized laser (632 nm) supplied by Melles Griot.

Dynamic Light Scattering (DLS). DLS measurements were performed on a Nanotrac Particle Size Analyzer (Microtrac Inc.).

RESULTS AND DISCUSSION

Graphene used in this study was obtained by two different methods: thermal treatment of graphite oxide and liquid-phase exfoliation of graphite.[20,21]

Four aqueous graphene dispersions exhibiting different degrees of exfoliation and stability were prepared with the aid of sonication. Dispersions A, A-LC (LC standing for low concentration), and A-HE (HE standing for high energy) were prepared from graphene, produced by thermal reduction of graphite oxide.[20] Dispersions A and A-HE were prepared under similar conditions, meaning that the same energy was provided to both systems during the sonication process (Table 1). The differences between those two are the graphene and surfactant concentrations [1 mg mL^{-1} and 1:1 graphene:sodium cholate (SC) weight ratio and 0.1 mg mL^{-1} and 1:1 graphene:SC weight ratio for dispersion A and dispersion A-HE, respectively], meaning that dispersion A-HE was exposed to a 10-fold larger amount of energy per graphene unit than dispersion A. Dispersion A-LC with a graphene concentration of 0.1 mg mL^{-1} and a 1:1 graphene:SC ratio was exposed to a 10-fold smaller amount of energy than dispersions A and A-HE. This implies that the absorbed amount of energy per graphene unit was the same as in the case of sample A and 10-fold smaller than for sample A-HE. Dispersion B was prepared from graphene produced by the liquid-phase exfoliation of graphite. Graphene for dispersion B did not have to be sonicated additionally, because it had been obtained in the form of a stable aqueous solution after sonication of graphite at a concentration of 5 mg mL^{-1} in a 0.1 mg mL^{-1} solution of SC for 100 h, followed by centrifugation, resulting in a final graphene concentration of 0.1 mg mL^{-1}.[21] We note that the concentration of surfactant in all four dispersions is far below the critical micelle concentration (~5 mg mL^{-1}). The choice of the surfactant concentrations is based on a study reported elsewhere, which demonstrated that in the applied range of concentrations the surfactant provides a higher stability to the dispersed graphene than at the concentrations close to the critical micelle concentration.[21]

Table 1. Graphene Dispersions Used for the Preparation of Composites

sample	concn (mg mL^{-1})	energy provided during sonication (J)	added amount of energy per milligram of graphene (J)
A	1	2200000	22000
A-LC	0.1	220000	22000
A-HE	0.1	2200000	220000
B	0.1	–	–

The two different kinds of graphene used in this study were characterized by Raman spectroscopy. The 633 nm Raman

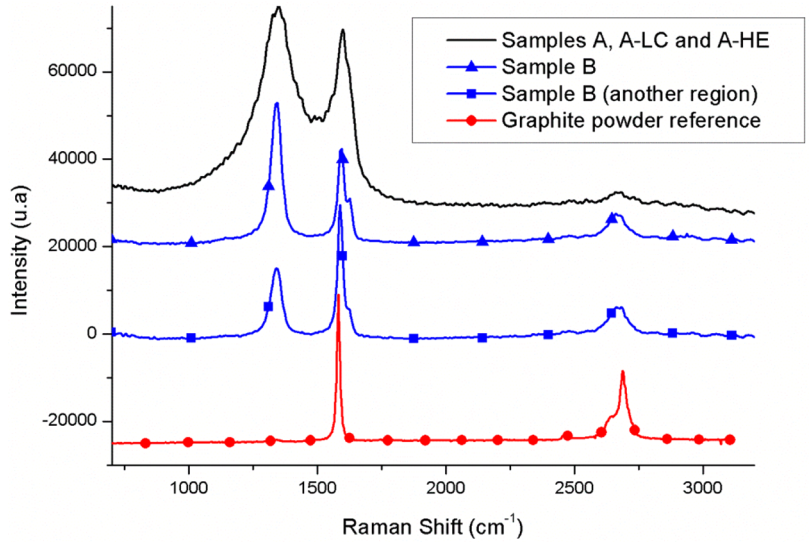

Figure 1. Raman spectra of graphene used for preparation of the aqueous dispersions.

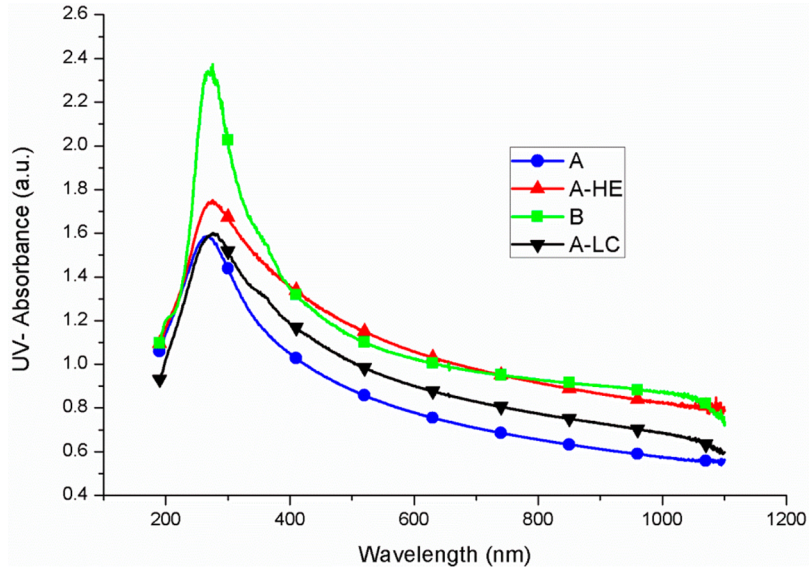

Figure 2. UV−vis spectra of aqueous dispersions A (2200000 J), A-LC (220000 J), A-HE (2200000 J), and B.

spectra of graphene and bulk graphite are compared in Figure 1. The two most intense features for graphite are the *G* peak at ∼1575 cm^{-1} and the 2*D* peak at ∼2681 cm^{-1}. The *G* band represents a tangential shear mode of carbon atoms that corresponds to the stretching mode in the graphite plane. The *G* peak is due to the doubly degenerate zone center mode.[22] The 2*D* band has nothing to do with the *G* peak but represents a second-order process from two-zone boundary longitudinal optical phonons. It is an intrinsic property of graphite, and present even in defect-free structures. Because zone-boundary phonons do not satisfy the fundamental Raman selection rule, they are not seen in first-order Raman spectra of defect-free graphite. Such phonons give rise to a peak at ∼1350 cm^{-1} in defect-containing graphite, called the *D* peak.[23]

The conventional Raman spectrum of graphite and graphene layers has been studied in great detail by Ferrari et al.[23] Graphene shows a Raman spectrum very similar to that of graphite, and the differences observed mirror the missing interaction between the layers. The 2*D* peak (second-order) changes in shape, width, and position with an increasing number of layers, reflecting the change in the electron bands via a double-resonant Raman process. The *G* peak should exhibit slight shifts in position and a great decrease in the peak intensity of the *G*/2*D* ratio.

The spectra in Figure 1 show a significant change in the shape and intensity of the 2*D* peak of graphene compared to the shape and intensity of that of bulk graphite. The 2*D* peak in bulk graphite presents a shoulder with roughly one-fourth of the height of the *G* peak followed by a main peak. For graphene sample B, a single 2*D* peak that is slightly shifted to lower wavelengths can be observed. The intensity of the peak is never higher than that obtained for the *G* peak. We note that all graphene spectra have *D* bands significantly more intense than that of the graphite powder, indicating that processing, more specifically sonication, induces defects. We can divide such defects into two main types: body defects, such as point defects on the basal plane, and edge defects. The introduction of edge defects is unavoidable during processing as sonication cuts the

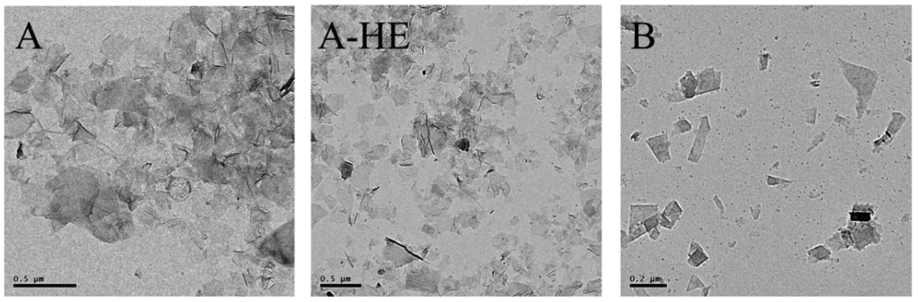

Figure 3. TEM pictures of aqueous graphene/SC dispersions A, A-HE, and B. A droplet of each dispersion was deposited on a carbon grid for analysis.

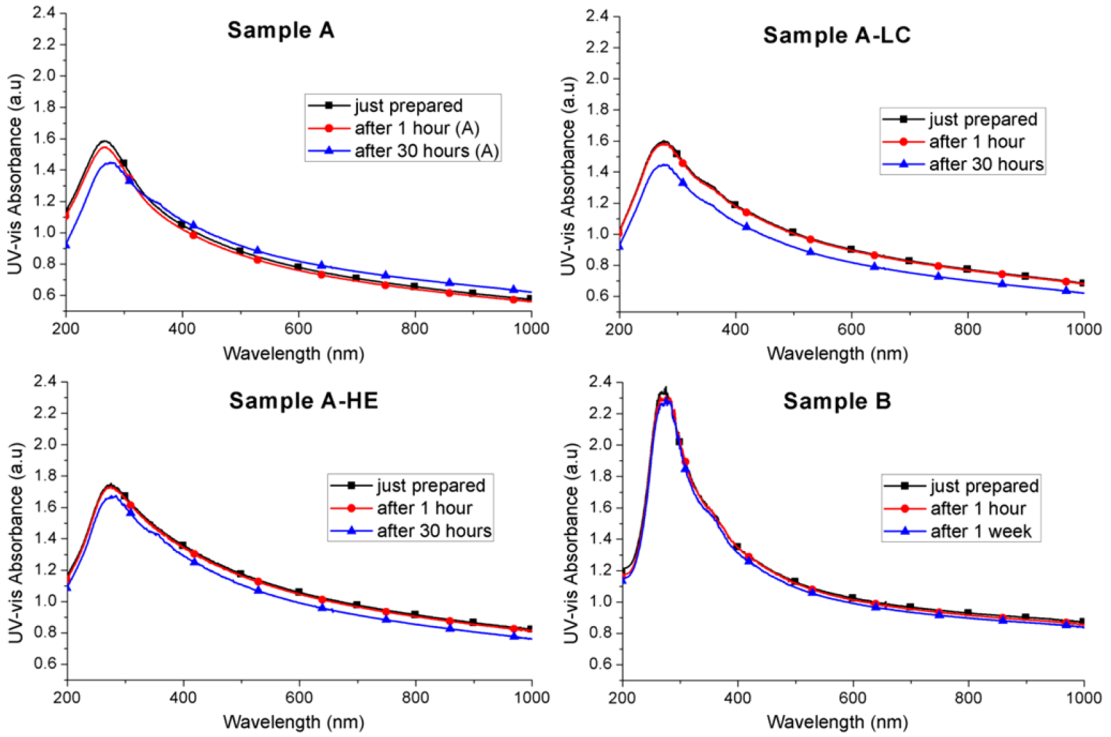

Figure 4. Stability of systems A, A-LC, A-HE, and B recorded over time by UV−vis spectroscopy.

initially large crystallites up into smaller flakes. These smaller flakes have more edges per unit mass, resulting in an increase in the edge defect population.[21] For graphene samples A, A-LC, and A-HE, no clear 2*D* peak can be identified. Chemical modifications like oxidation and reduction can lead to even more severe structural damage to the surface of these materials, introducing defects that may disrupt the band structure. The broadness and high intensity of the defect *D* peak for samples A, A-LC, and A-HE confirm this assumption.

During the sonication process, the increasing number of exfoliated graphene platelets results in an increase in UV−vis absorbance due to an increase in the surface area of graphene; the process also prevents particle sedimentation.[24−28]

As one can see in Figure 2, the final aqueous dispersions exhibit different UV−vis absorbances and hence different degrees of graphene exfoliation. The highest absorbance spectrum corresponds to dispersion B, whereas dispersions A, A-LC, and A-HE exhibit lower absorbance spectra, which means that dispersion B contains the largest number of thin graphene layers in comparison with dispersions A, A-LC, and A-HE, which in turn contain a larger number of agglomerates. Upon comparison of samples A, A-LC, and A-HE, one can conclude that apparently samples A and A-LC have more agglomerates than sample A-HE, which is in line with the amount of energy supplied to A and A-LC being smaller than the amount supplied to A-HE. Sample A in turn looks just slightly more agglomerated than sample A-LC, but the difference is very small, which makes sense in view of the similar amount of energy supplied per milligram of of graphene in both systems A and A-LC. Visually, both dispersions A-HE and B are stable for a few weeks and months, respectively, whereas in dispersions A and A-LC, slight sedimentation occurs within 24 h of preparation.

All dispersion samples were visually stable, showing no indication of sedimentation. The corresponding TEM images (Figure 3) of the graphene platelets obtained by using the processing conditions described above (samples A, A-HE, and B) displayed some difference in size between the samples.

Platelets obtained for dispersion A are slightly larger than those obtained for dispersions A-HE and B. This must be due to the different amounts of energy provided per milligram of graphene during the sonication process. As one can see from

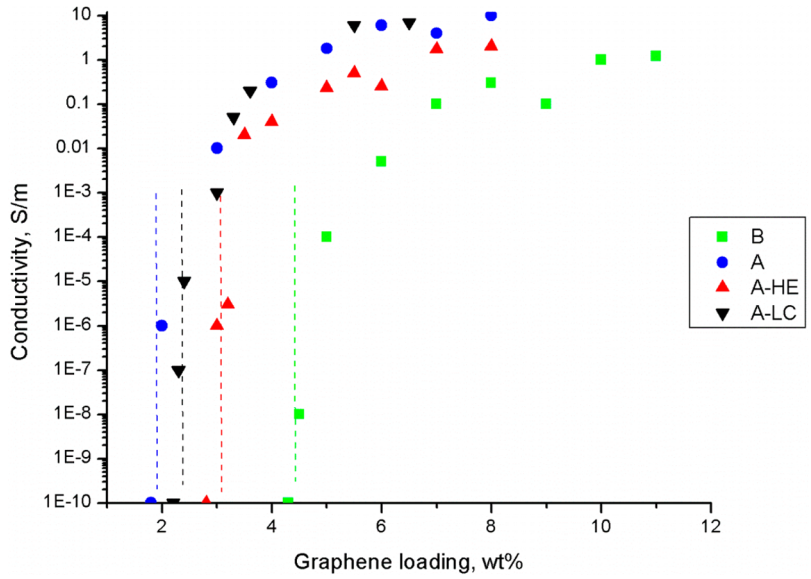

Figure 5. Electrical conductivity of graphene/PS composites A, A-LC, A-HE, and B, prepared with aqueous dispersions A, A-LC, A-HE, and B, respectively, as a function of graphene weight fraction in the final nanocomposite.

Figure 4, the maximal absorbance around 270 nm of both dispersions A and A-LC, which had an almost similar degree of exfoliation just after the sonication process, decreases markedly over time, which in all likelihood is due to relatively fast aggregation occurring in both dispersions. During the same period of time, there is a very slight decrease in the absorbance of sample A-HE, suggesting that dispersion A-HE exhibits a stability higher than those of dispersions A and A-LC. Sample B shows hardly any decrease in its UV−vis absorbance maximum around 275 nm over long periods of time, indicating an extremely high stability of the dispersion and no aggregation processes occurring.

All four graphene/SC dispersions, A, A-LC, A-HE, and B, were utilized for the preparation of conductive polymer nanocomposites via the so-called latex technology. For that, the aqueous graphene/SC dispersions were mixed with polystyrene latex, followed by freeze-drying and compression molding, resulting in a composite film.[7] Hereafter, the composites prepared from graphene dispersions A, A-LC, A-HE, and B and PS latex are indicated as nanocomposites A, A-LC, A-HE, and B, respectively.

The electrical conductivity of the nanocomposites as a function of the nanofiller content is shown in Figure 5. It is known that compression molding may induce particle orientation.[11,29] Therefore, there is a difference in conductivity for the surface (in-plane) direction compared to the transverse (through-the-sample) direction. In this work, for the sake of comparison, the conductivities for all composite samples were measured in the surface (in-plane) direction.

At low graphene concentrations, as long as no conductive network of nanoplatelets is formed in the PS matrix, the conductivity of the nanocomposites remains very close to the conductivity value of the pure insulating PS matrix. The figure clearly shows that the percolation thresholds vary quite strongly with dispersion conditions. The percolation threshold of the composites prepared from dispersion B is high, ∼4.5 wt %, which is related to the fact that graphene platelets stay separated one from another in the final composite films just as they were in the aqueous mixture of the PS latex and the graphene dispersion because of the very high degree of exfoliation and high stability, which brings about a lack of contacts between them. The nanocomposites obtained from dispersion A-HE show a moderate percolation threshold in comparison with that of composites based on graphene dispersions B, presumably due to the lower degree of exfoliation of the platelets, the reduced thermodynamic stability of the dispersion, and hence the presence of small agglomerates. The attractive interactions leading to the agglomerates plausibly induce additional contacts between sheets in the aqueous graphene/PS particle mixtures and hence subsequently also in the composite films.

The nanocomposites based on graphene dispersions A and A-LC exhibit the lowest percolation thresholds, viz., 2 wt % for A and 2.3 wt % for A-LC, because of their relatively low degrees of exfoliation and significantly reduced stability of the aqueous dispersions compared to the values in the cases discussed above. This results in some agglomeration and hence cluster formation in the aqueous graphene/polymer particle mixtures and, following that, in the solid composite, too. We emphasize that we are not dealing here with the worst possible scenario concerning the dispersed state of graphene, which would be the case for completely nonexfoliated graphite in the polymer matrix for which the percolation threshold experimentally proved to occur at a very high filler loading, viz., 10 wt %. When the composites are made from nonexfoliated graphite, then because of macroscopic phase separation, there might be isolated graphite-rich regions along with a vast majority of composite volume that would be largely unreinforced and polymer-rich.

The organization of graphene sheets in the nanocomposites and their conductivity distribution was analyzed with nanometer resolution by means of conductive atomic force microscopy (C-AFM). Using a conductive AFM probe, in this case a gold-coated silicon tip, the local electrical conductivity was measured at exactly the same area of the specimen subsequent to the topography and phase contrast imaging. The C-AFM tip measures the current throughout the volume of the nanocomposite specimen at a given voltage, which is running via the graphene network to the ground contacts. Only platelets that are connected with the ground

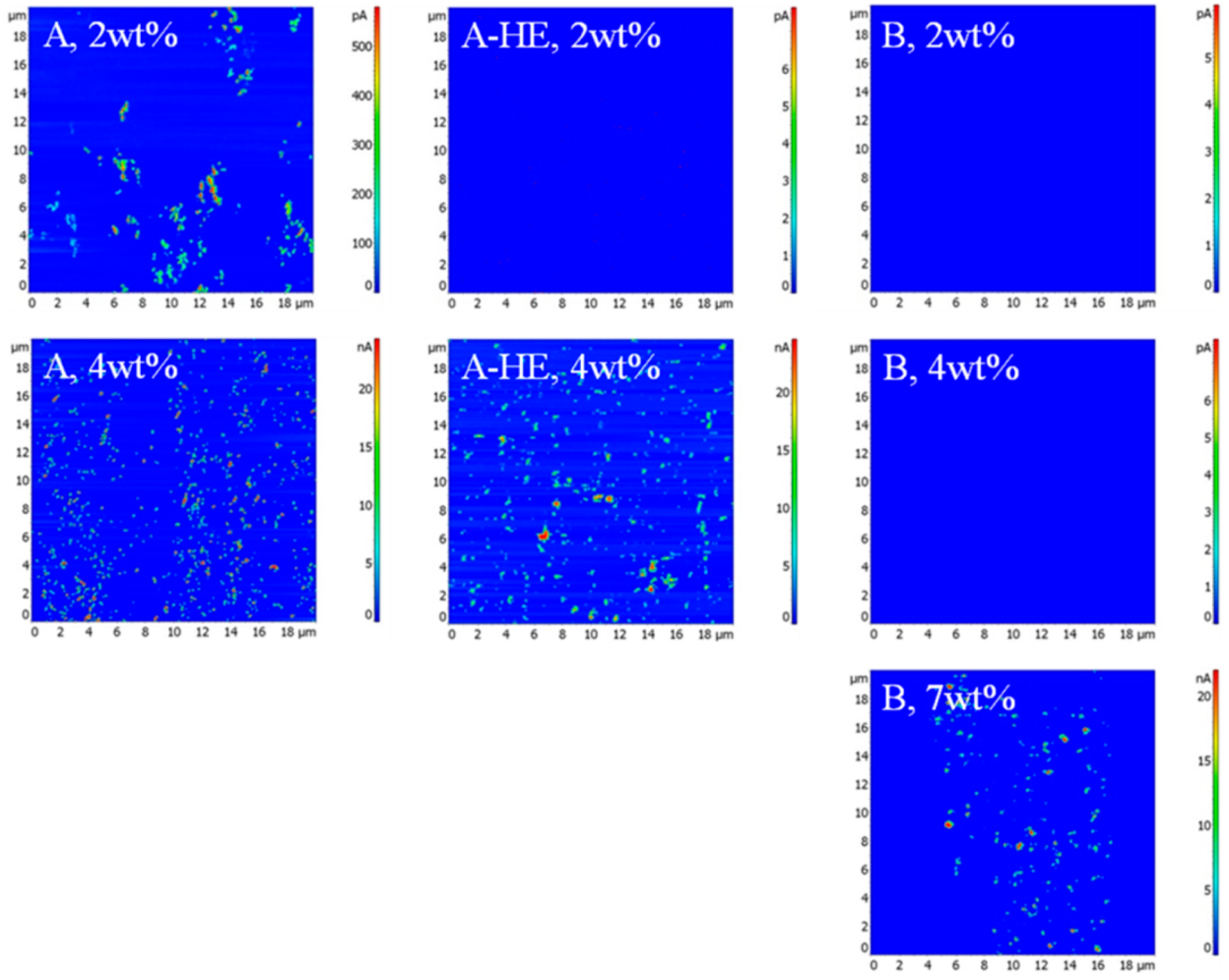

Figure 6. Conductive AFM images of the graphene/PS nanocomposites with different graphene loadings (indicated in the pictures) obtained as electrical current distribution images showing the graphene platelets that are connected with the ground electrode.

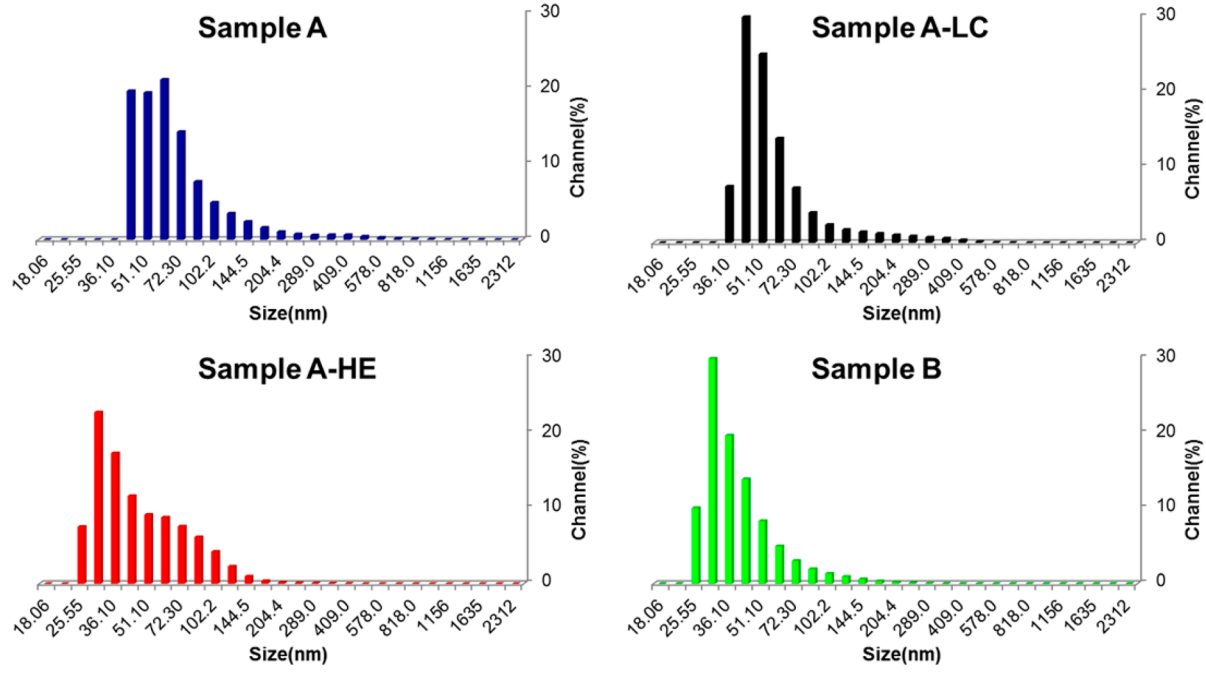

Figure 7. Dynamic light scattering data of the size distributions of aqueous graphene dispersions A, A-LC, A-HE, and B.

contacts can be monitored, and the observed differences in current are determined by the intranetwork graphene junctions with the highest resistivity. Graphene contributing to subnetworks without connection to the ground contacts shows no current. In this way, a current distribution image is obtained and the conductive platelets can be distinguished from the insulating polymer matrix.

As one can see in Figure 6 at 2 wt % graphene loading, only nanocomposite A that shows some small conductive clusters exhibits some degree of conductivity, whereas both samples A-HE and B do not. At a higher loading, 4 wt %, both samples prepared from graphene dispersions A and A-HE show conductivity, but samples B still do not exhibit any network formation. Finally, at 7 wt % loading, a conductive network is easily visible in nanocomposite sample B, as well.

We also employed DLS to obtain a rough indication of the size distributions in the exfoliated aqueous graphene/SC dispersions (Figure 7). Because DLS analysis assumes that the measured objects are spherical in shape, whereas graphene platelets can be more accurately described as two-dimensional objects, the data obtained from DLS measurements are not the real dimensions of the platelets but rather the effective hydrodynamic diameter of an equivalent sphere described by tumbling platelets.[30] The object does not need to be spherical to have an apparent hydrodynamic radius or diameter.

From the DLS measurements, the dispersions turned out to have quite some variation in their size distributions with a difference in the average values as well as a difference in the thickness of the tail of the distribution for large sheets. To rationalize these experimental observations, we attempt to assess whether the difference in the percolation thresholds could be explained by the variations in the size distributions. For this, we make use of a recently formulated connectivity percolation theory that predicts the effect on the percolation threshold of a size polydispersity of impenetrable and rigid platelike particles.[31] It is worth noting that our study is based on the presumption of thermodynamic equilibrium, where we stress that aggregation does not need to be an out-of-equilibrium process as long as macroscopic phase separation is not favored. Our theory can and does handle equilibrium clusters, though in our curve fitting we did not consider any net attraction between the sheets. Gelation by strong attractive forces gives rise to rigidity percolation, which is different from what we study, geometric percolation. Reduced thermodynamic stability in this context means a propensity for phase separation between sheets and polymer matrix, even though the driving force might not be strong enough to actually produce phase separation. The theory presumes charge transport to take place via electron hopping if two neighboring particles are sufficiently close to each other and predicts a very sensitive dependence of the percolation threshold on the shape of the size distribution of the platelike particles.

Interestingly, the threshold turned out to depend only on a number of higher-order moments of the full size distribution function, in particular the skewness of the distribution, allowing us to apply this model straightforwardly to the distribution data we obtained from the DLS measurements. This means that we compute the critical volume fraction φ_p of graphene required to obtain a system-spanning network as given by eq 24 of ref 31 that reads

$$\phi_p = 4\langle L_k D_\gamma^2\rangle_{k\gamma}\frac{B - \sqrt{B^2 - C}}{\lambda C}$$

with

$$B = 4(\pi + 5)\langle L_k D_\gamma\rangle_{k\gamma} + (5\pi + 6)\langle D_\gamma^2\rangle_\gamma + (7\pi + 16)\lambda \langle D_\gamma\rangle_\gamma$$

and

$$C = (\pi + 6)[-16\pi\langle D_\gamma\rangle_\gamma\langle D_\gamma^3\rangle_\gamma - (\pi + 6)\langle D_\gamma^4\rangle_\gamma + (17\pi + 6)\langle D_\gamma^2\rangle_\gamma^2]$$

where the angle brackets denote an average over the distribution of thicknesses L_k and diameters D_γ. This volume fraction φ_p is then converted into a weight fraction using a conversion factor of 2, because the density of graphene is twice that of the polymer. To determine the required moments of the distribution, we presume the thickness of the graphene sheets to be a constant and, hence, the diameter and thickness distribution to be independent. This may be a tenuous approximation because one might expect that because of the sonication process the probability of a thinner sheet to break up into smaller ones is larger than that of a thicker one. However, the problem of invoking both diameter and thickness is that we need access to information about the covariants of the diameter and thickness distribution function. This information is not available and to the best of our knowledge has never been investigated experimentally. If we presume width and thickness to be independent, which actually is highly unlikely because of sonication, then it turns out that the effect of diameter polydispersity is very much stronger than that of thickness polydispersity. In fact, eq 26 of ref 31 shows that information about the thickness is absorbed in λ, the connectivity range, which incidentally in principle also depends on the thickness and diameter of the particles. Therefore, as stated above, because of a lack of information about the coupling of the distributions, we use this approximation that should allow us to assess whether the discrepancies in the observed percolation thresholds are caused by a polydispersity in the diameters. Within the goals of our study, ignoring the thickness polydispersity is, in our view, justified.

Given the distributions of diameters, there are two tunable parameters in the model, the sheet thickness L and the hopping distance λ, which is the largest separation between two particles that still allows a charge carrier to hop from one graphene sheet to the other. Because of the strong tendency of the particles to stick together, they may in fact consist of multiple layers of graphene instead of a single layer. Hence, we take three values of the thickness to mimic a single graphene layer (L = 0.3 nm), three layers (L = 1.0 nm), and six layers (L = 2.0 nm) to which to compare our experimental results. For each of these values, we fit the hopping distance for the average experimental value, i.e., that of dispersion A-HE with an experimentally determined percolation threshold of 3.0 wt %, and the obtained value of λ we use to determine the theoretical threshold for the other dispersions. The results are listed in Table 2.

We observe that the choice of a larger value of sheet thickness increases the value of the hopping distance that is required for an accurate fit of the experimental data; i.e., λ = 4.5 nm for L = 1.0 nm, and λ = 8.5 nm for L = 2.0 nm. This is because from the model it follows that a large thickness increases the percolation threshold, whereas a larger hopping distance decreases it.[26] Surprisingly, there is little variation in the results, and for all three choices of thickness, the agreement between theory and experiment is quite good, considering the

Table 2. Experimentally Determined Percolation Thresholds for PS/Graphene Nanocomposites Based on the Four Aqueous Graphene Dispersions (A, A-LC, A-HE, and B) and the Corresponding Theoretical Predictions for Different Values of Graphene Thickness L and Hopping Distance λ

	A (wt %)	A-HE (wt %)	A-LC (wt %)	B (wt %)
experiment	2.0	3.0	2.3	4.5
theory (L = 0.3 nm; λ = 1.4 nm)	2.1	3.0	2.6	2.8
theory (L = 1.0 nm; λ = 4.6 nm)	2.2	3.0	2.7	2.8
theory (L = 2.0 nm; λ = 8.5 nm)	2.3	3.0	2.8	2.8

crudeness of the model. Indeed, for the three chosen values of plate thickness L, the trends fully agree and the numerical agreement between theory and experiment is almost perfect for composites A, A-HE, and A-LC, but the value for the experimental value of composite B is underestimated in all cases. From the fitting procedure, we find quite different values for the hopping distance, the exact value of which is not known accurately. As already mentioned, the value of platelet thickness is not known accurately either and may be different for the different dispersions. Indeed, nanocomposite B shows the highest UV absorbance and therefore has the highest degree of exfoliation. This means that the sheets in dispersion B are presumably thinner than those in the other three dispersions and that L = 0.3 nm is quite accurate for dispersion B but may be too low for the other three systems, so for these, the value L = 1 nm or L = 2 nm may be more realistic. An interesting point to note here is that the graphene sheets are modeled as flat disks in the model, which obviously they are not. For the theory, the precise shape has relatively little impact as long as the object is flat, and its thickness is much shorter than its width. Hence, we focused on simplicity on size and modeled the sheets as perfect disks. Indeed, if the sheets in aqueous graphene dispersion B are thinner than those in the other three dispersions because of the higher degree of exfoliation, their effective diameter as observed in the DLS measurements should be smaller, which in fact is the case. The diameter in the model then represents this effective sheet diameter, which leads to a good agreement between experiment and theory for the PS/graphene nanocomposite based on this dispersion.

As already mentioned, the value of the hopping distance is not known accurately, but values of 4.6 and 8.5 nm that we found to fit the data may be quite large.[32] A smaller value of this typical distance over which charge transport occurs would lead to a higher percolation threshold, but the trend in them remains correct. This means that there could be a systematic deviation in the theoretical predictions, which could, e.g., be due to attractive van der Waals interactions that are not identified in the model and have been shown to lower the percolation threshold of carbon nanotubes in a PS matrix considerably.[32] Here, it must be noted that the attraction should not be too large because that would lead to stacking of sheets (or bundling of nanotubes), which would increase the percolation threshold of the PS/graphene nanocomposite. Therefore, if the effect of such a systematic deviation in nanocomposites A, A-LC, and B is the same, then we could argue that the differences between their percolation thresholds are indeed related to the polydispersities of their sheet diameters.

CONCLUSIONS

Both experimental and theoretical studies were applied to determine an effect of the dispersion state on the percolation threshold of graphene-based polystyrene nanocomposites prepared with the aid of latex technology. Graphene/polystyrene composites were prepared using four graphene dispersions with different degrees of exfoliation and stability, and their electrical properties were characterized.

The degree of exfoliation of graphene and the stability of the dispersions were characterized with UV−vis spectroscopy. It was shown that PS/graphene nanocomposites prepared from PS latex and aqueous graphene dispersions with relatively low stability and relatively low degrees of exfoliation exhibit a percolation threshold lower than that of the composites based on dispersions with a higher degree of graphene exfoliation and higher dispersion stability.

Theoretical predictions were employed to calculate percolation thresholds of the nanocomposites, inserting the degree of polydispersity of the graphene platelets as obtained from our DLS measurements. Theory and experiments show the same trends for the series of samples for the three choices of particle thickness (i.e., L = 0.3, 1.0, and 2.0 nm), suggesting that size polydispersity is indeed an important factor determining the electrical percolation threshold. These different values of L give rise to different values for the hopping distance, but this leaves the trend in the percolation threshold unaffected. With regard to these thicknesses, nanocomposite B shows a higher degree of exfoliation, both in the aqueous state and in the final nanocomposite, and a stability higher than that in the other composites that exhibit cluster formation. This means that the particles in composite B are presumably somewhat thinner than those in the other composites.

Despite the higher quality of the nanofiller loading of composite B, confirmed by Raman spectroscopy, nanocomposites based on lower-quality aqueous dispersions of graphene, but in which the nanofiller particles do form clusters in solution, and accordingly in view of our mild and almost shear-free compression molding step furnishing the nanocomposite films, also in the final PS/graphene nanocomposite, exhibit lower percolation thresholds. This important finding, to the best of our knowledge demonstrated for the first time for graphene-based polymer nanocomposites, is in excellent agreement with the works described by Li, Martin, Aguilar, and Hernandez on polymer/carbon nanotube composites.[12−15]

AUTHOR INFORMATION

Corresponding Author

*E-mail: p.vanderschoot@phys.tue.nl. Telephone: +31.402474347. Fax: +31.402445253.

Notes

The authors declare no competing financial interest.

ACKNOWLEDGMENTS

This work is part of the Research Program of the Dutch Polymer Institute (DPI), Project 648.

REFERENCES

(1) Allen, M. J.; Tung, V. C.; Kaner, R. B. Honeycomb Carbon: A Review of Graphene. *Chem. Rev.* **2010**, *110* (1), 132−145.

(2) Kim, H.; Abdala, A. A.; Macosko, C. W. Graphene/Polymer Nanocomposites. *Macromolecules* **2010**, *43* (16), 6515−6530.

(3) Ghislandi, M.; Tkalya, E.; Schillinger, S.; Koning, C. E.; de With, G. High Performance Graphene- and MWCNTs-based PS/PPO Composites Obtained via Organic Solvent Dispersion. *Compos. Sci. Technol.* **2013**, *80*, 16−22.
(4) Stankovich, S.; Dikin, D. A.; Dommett, G. H. B.; Kohlhaas, K. M.; Zimney, E. J.; Stach, E. A.; Piner, R. D.; Nguyen, S. T.; Ruoff, R. S. Graphene-based Composite Materials. *Nature* **2006**, *442* (7100), 282−286.
(5) Eda, G.; Fanchini, G.; Chhowalla, M. Large-area Ultrathin Films of Reduced Graphene Oxide as a Transparent and Flexible Electronic Material. *Nat. Nanotechnol.* **2008**, *3* (5), 270−274.
(6) Ghislandi, M. Nano-scaled Carbon Fillers and their Functional Polymer Composites. Ph.D. Thesis, Eindhoven University of Technology: Eindhoven, The Netherlands, 2012.
(7) Tkalya, E.; Ghislandi, M.; Alekseev, A.; Koning, C.; Loos, J. Latex-based Concept for the Preparation of Graphene-based Polymer Nanocomposites. *J. Mater. Chem.* **2010**, *20* (15), 3035−3039.
(8) Kim, H.; Miura, Y.; Macosko, C. W. Graphene/Polyurethane Nanocomposites for Improved Gas Barrier and Electrical Conductivity. *Chem. Mater.* **2010**, *22* (11), 3441−3450.
(9) Javier, S. H.; Martinez, G.; Gomez, M. A. Synthesis of Poly(vinyl alcohol)/reduced Graphite Oxide Nanocomposites with Improved Thermal and Electrical Properties. *J. Mater. Chem.* **2009**, *19* (28), 5027−5032.
(10) Kim, H.; Macosko, C. W. Processing-property Relationships of Polycarbonate/graphene Composites. *Polymer* **2009**, *50* (15), 3797−3809.
(11) Ghislandi, M.; Tkalya, E.; Marinho, B.; Koning, C. E.; de With, G. Electrical Conductivities of Carbon Powder Nanofillers and their Latex-based Polymer Composites. *Composites, Part A* **2013**, *53*, 145−151.
(12) Li, J.; Ma, P. C.; Chow, W. S.; To, C. K.; Tang, B. Z.; Kim, J. K. Correlations between Percolation Threshold, Dispersion State, and Aspect Ratio of Carbon Nanotubes. *Adv. Funct. Mater.* **2007**, *17* (16), 3207−3215.
(13) Martin, C. A.; Sandler, J. K. W.; Shaffer, M. S. P.; Schwarz, M. K.; Bauhofer, W.; Schulte, K.; Windle, A. H. Formation of Percolating Networks in Multi-wall Carbon-nanotube-epoxy Composites. *Compos. Sci. Technol.* **2004**, *64* (15), 2309−2316.
(14) Hernandez, J. J.; Garcia-Gutierrez, M. C.; Nogales, A.; Rueda, D. R.; Kwiatkowska, M.; Szymczyk, A.; Roslaniec, Z.; Concheso, A.; Guinea, I.; Ezquerra, T. A. Influence of Preparation Procedure on the Conductivity and Transparency of SWCNT-polymer Nanocomposites. *Compos. Sci. Technol.* **2009**, *69* (11−12), 1867−1872.
(15) Aguilar, J. O.; Bautista-Quijano, J. R.; Aviles, F. Influence of Carbon Nanotube Clustering on the Electrical Conductivity of Polymer Composite Films. *eXPRESS Polym. Lett.* **2010**, *4* (5), 10.
(16) Regev, O.; ElKati, P. N. B.; Loos, J.; Koning, C. E. Preparation of Conductive Nanotube-polymer Composites Using Latex Technology. *Adv. Mater.* **2004**, *16* (3), 248−251.
(17) Grossiord, N.; Loos, J.; Regev, O.; Koning, C. E. Toolbox for Dispersing Carbon Nanotubes into Polymers To Get Conductive Nanocomposites. *Chem. Mater.* **2006**, *18* (5), 1089−1099.
(18) Yu, J.; L, K.; Sourty, E.; Grossiord, N.; Koning, C.; Loos, J. Characterization of Conductive Multiwall Nanotube/polystyrene Composites Prepared by Latex Technology. *Carbon* **2007**, *45*, 2897−2903.
(19) Tkalya, E. E.; Ghislandi, M.; de With, G.; Koning, C. E. The Use of Surfactants for Dispersing Carbon Nanotubes and Graphene to Make Conductive Nanocomposites. *Curr. Opin. Colloid Interface Sci.* **2012**, *17* (4), 225−231.
(20) McAllister, M. J.; Li, J. L.; Adamson, D. H.; Schniepp, H. C.; Abdala, A. A.; Liu, J.; Herrera-Alonso, M.; Milius, D. L.; Car, R.; Prud'homme, R. K.; Aksay, I. A. Single Sheet Functionalized Graphene by Oxidation and Thermal Expansion of Graphite. *Chem. Mater.* **2007**, *19* (18), 4396−4404.
(21) Lotya, M.; King, P. J.; Khan, U.; De, S.; Coleman, J. N. High-Concentration, Surfactant-Stabilized Graphene Dispersions. *ACS Nano* **2010**, *4* (6), 3155−3162.
(22) Tuinstra, F.; Koenig, J. L. Raman Spectrum of Graphite. *J. Chem. Phys.* **1970**, *53* (3), 1126.
(23) Ferrari, A. C.; Meyer, J. C.; Scardaci, V.; Casiraghi, C.; Lazzeri, M.; Mauri, F.; Piscanec, S.; Jiang, D.; Novoselov, K. S.; Roth, S.; Geim, A. K. Raman Spectrum of Graphene and Graphene Layers. *Phys. Rev. Lett.* **2006**, *97* (18), 187401.
(24) Grossiord, N.; Regev, O.; Loos, J.; Meuldijk, J.; Koning, C. E. Time-dependent Study of the Exfoliation Process of Carbon Nanotubes in Aqueous Dispersions by Using UV-visible Spectroscopy. *Anal. Chem.* **2005**, *77* (16), 5135−5139.
(25) Stankovich, S.; Piner, R. D.; Chen, X. Q.; Wu, N. Q.; Nguyen, S. T.; Ruoff, R. S. Stable Aqueous Dispersions of Graphitic Nanoplatelets via the Reduction of Exfoliated Graphite Oxide in the Presence of Poly(sodium 4-styrenesulfonate). *J. Mater. Chem.* **2006**, *16* (2), 155−158.
(26) Jiang, L. Q.; Gao, L.; Sun, J. Production of Aqueous Colloidal Dispersions of Carbon Nanotubes. *J. Colloid Interface Sci.* **2003**, *260* (1), 89−94.
(27) Ryabenko, A. G.; Dorofeeva, T. V.; Zvereva, G. I. UV-VIS-NIR Spectroscopy Study of Sensitivity of Single-wall Carbon Nanotubes to Chemical Processing and Van-der-Waals SWNT/SWNT Interaction. Verification of the SWNT Content Measurements by Absorption Spectroscopy. *Carbon* **2004**, *42* (8−9), 1523−1535.
(28) Torrens, O. N.; Milkie, D. E.; Zheng, M.; Kikkawa, J. M. Photoluminescence from Intertube Carrier Migration in Single-walled Carbon Nanotube Bundles. *Nano Lett.* **2006**, *6* (12), 2864−2867.
(29) Marinho, B.; Ghislandi, M.; Tkalya, E.; Koning, C. E.; de With, G. Electrical Conductivity of Compacts of Graphene, Multi-wall Carbon Nanotubes, Carbon Black, and Graphite Powder. *Powder Technol.* **2010**, *221*, 351−358.
(30) Stankovich, S.; Piner, R. D.; Nguyen, S. T.; Ruoff, R. S. Synthesis and Exfoliation of Isocyanate-treated Graphene Oxide Nanoplatelets. *Carbon* **2006**, *44* (15), 3342−3347.
(31) Otten, R. H. J.; van der Schoot, P. Connectivity Percolation of Polydisperse Anisotropic Nanofillers. *J. Chem. Phys.* **2011**, *134* (9), 094902.
(32) Kyrylyuk, A. V.; van der Schoot, P. Continuum Percolation of Carbon Nanotubes in Polymeric and Colloidal Media. *Proc. Natl. Acad. Sci. U.S.A.* **2008**, *105* (24), 8221−8226.